

1 Satellite-based Estimation of the Impacts of Summertime Wildfires on
2 Particulate Matter Air Quality in United States

3 Zhixin Xue¹, Pawan Gupta^{2,3}, and Sundar Christopher¹

4 ¹Department of Atmospheric and Earth Science, The University of Alabama in Huntsville,
5 Huntsville, 35806 AL, USA

6 ²STI, Universities Space Research Association (USRA), Huntsville, 35806 AL, USA

7 ³NASA Marshall Space Flight Center, Huntsville, AL, 35806, USA

8 **Abstract**

9 Frequent and widespread wildfires in North Western United States and Canada has become
10 the “*new normal*” during the northern hemisphere summer months, which significantly degrades
11 particulate matter air quality in the United States ~~significantly~~. Using the mid-visible Multi Angle
12 Implementation of Atmospheric Correction (MAIAC) satellite-derived Aerosol Optical Depth
13 (AOD) with meteorological information from the European Centre for Medium-Range Weather
14 Forecasts (ECMWF) and other ancillary data, we quantify the impact of these fires on fine
15 particulate matter (PM2.5) air quality in the United States. We use a Geographically Weighted
16 Regression method to estimate surface PM2.5 in the United States between low (2011) and high
17 (2018) fire activity years. Our results indicate that smoke aerosols caused significant pollution
18 changes over half of the United States. We estimate that nearly 29 states have increased PM2.5
19 during the fire active year and 15 of these states have PM2.5 concentrations more than 2 times
20 than that of the inactive year. Furthermore, these fires increased daily mean surface PM2.5
21 concentrations in Washington and Oregon by 38 to 259 $\mu\text{g}\text{m}^{-3}$ posing significant health risks
22 especially to vulnerable populations. Our results also show that the GWR model can be

23 successfully applied to PM_{2.5} estimations from wildfires thereby providing useful information for
24 various applications including public health assessment.

25 **1. Introduction**

26 The United States (US) Clean Air Act (CAA) was passed in 1970 to reduce pollution levels
27 and protect public health that has led to significant improvements in air quality (Hubbell et al.,
28 2010; Samet, 2011). However, the northern part of the US continues to experience an increase in
29 surface PM_{2.5} due to fires in North Western United States and Canada (hereafter NWUSC)
30 especially during the summer months and these aerosols are a new source of ‘pollution’ (Coogan
31 et al., 2019; Dreessen et al., 2016). The smoke aerosols from these fires increase fine particulate
32 matter (PM_{2.5}) concentrations and degrade air quality in the United States (Miller et al., 2011).
33 Moreover several studies have shown that from 2013 to 2016, over 76% of Canadians and 69% of
34 Americans were at least minimally affected by wildfire smoke (Munoz-Alpizar et al., 2017).
35 Although wildfire pre-suppression and suppression costs have increased, the number of large fires
36 and the burnt areas in many parts of western Canada and the United States have also increased.
37 (Hanes et al., 2019; Tymstra et al., 2019). Furthermore, in a changing climate, as surface
38 temperature increases and humidity decreases, the flammability of land cover also increases, and
39 thus accelerate the spread of wildfires (Melillo et al., 2014). The accumulation of flammable
40 materials like leaf litter can potentially trigger severe wildfire events even in those forests that
41 hardly experience wildfires (Calkin et al., 2015; Hessburg et al., 2015; Stephens, 2005). .

42 Wildfire smoke exposure can cause small particles to be lodged in lungs that may lead to
43 exacerbations of asthma chronic obstructive pulmonary disease (COPD), bronchitis, heart disease
44 and pneumonia (Apte et al., 2018; Cascio, 2018). According to a recent study, a 10 μgm^{-3}
45 increase in PM_{2.5} is associated with a 12.4% increase in cardiovascular mortality (Kollanus et al.,

46 2016). In addition, exposure to wildfire smoke is also related to massive economic costs due to
47 premature mortality, loss of workforce productivity, impacts on the quality of life and
48 compromised water quality (Meixner and Wohlgemuth, 2004).

49 Surface PM_{2.5} is one of the most commonly used parameters to assess the health effects
50 of ambient air pollution. Given the sparsity of measurements in many parts of the world, it is not
51 possible to use interpolation techniques between monitors to provide PM_{2.5} estimate on a square
52 kilometer basis. Since surface monitors are limited, satellite data has been used with numerous
53 ancillary data sets to estimate surface PM_{2.5} at various spatial scales. Given the sparsity of
54 measurements in many parts of the world, it is not possible to use interpolation techniques between
55 monitors to provide PM_{2.5} estimate on a square kilometer basis. Several techniques have been
56 developed to estimate surface PM_{2.5} using satellite observations from regional to global scales
57 including simple linear regression, multiple linear regression, mixed-effect model, chemical
58 transport model (scaling methods), geographically weighted regression (GWR), and machine
59 learning methods (see Hoff and Christopher, 2009 for a review). The commonly used global
60 satellite data product is the 550nm (mid-visible) aerosol optical depth (AOD) which is a unitless
61 columnar measure of aerosol extinction (~~Wang and Christopher, 2006~~). Simple linear regression
62 method uses satellite AOD as the only independent variable, which shows limited predictability
63 compared to other method and correlation coefficients vary from 0.2 to 0.6 from the Western to
64 Eastern United States (Zhang et al., 2009). Multiple linear regression method uses meteorological
65 variables along with AOD data, and the prediction accuracy varies with different conditions
66 including the height of boundary layer and other meteorological conditions (Goldberg et al., 2019;
67 Gupta and Christopher, 2009b; Liu et al., 2005)(~~Liu, et al, 2005; Gupta and Christopher, 2009b~~).
68 For both univariate model and multi-variate models, AOD shows stronger correlation with PM_{2.5}

69 during-fire episodes compared to pre-fire and post-fire periods (Mirzaei et al., 2018). Chemistry
70 transport models (CTM) that scale the satellite AOD by the ratio of PM2.5 to AOD simulated by
71 models can provide PM2.5 estimations without ground measurements, which are different than
72 other statistical methods (Donkelaar et al., 2019, 2006). However, the CTM models that depend
73 on reliable emission data usually show limited predictability at shorter time scales, and is largely
74 useful for studies that require annual averages (Hystad et al., 2012).

75 The relationship among PM2.5, AOD and other meteorological variables is not spatially
76 consistent (Hoff and Christopher, 2009; Hu, 2009). Therefore, methods that consider spatial
77 variability can replicate surface PM2.5 with higher accuracy. One such method is the GWR, which
78 is a non-stationary technique that models spatially varying relationships by assuming the
79 coefficients in the model are functions of locations (Brunsdon et al., 1996; Fotheringham et al.,
80 1998, 2003). In 2009, satellite-retrieved AOD was introduced in the GWR method to predict
81 surface PM2.5– (Hu, 2009) followed by the use of meteorological parameters and land use
82 information (Hu et al., 2013). Several studies (Guo et al., 2021; Ma et al., 2014; You et al., 2016)
83 successfully applied GWR model in estimating PM2.5 in China by using AOD and meteorological
84 features as predictors. Similar to all the statistical methods, however, the GWR relies on adequate
85 number and density of surface measurements (Chu et al., 2016; Gu, 2019; Guo et al., 2021),
86 underscoring the importance of adequate ground monitoring of surface PM2.5.

87 In this paper, we use satellite data from the Moderate Resolution Imaging
88 Spectroradiometer (MODIS) and surface PM2.5 data combined with meteorological and other
89 ancillary information to develop and use the GWR method to estimate PM2.5. The use of the GWR
90 method is not novel and we merely use a proven method to apply this towards surface PM2.5
91 estimations for forest fires. We calculate the change in PM2.5 between a high fire activity (2018)

92 with low fire activity (2011) periods during summer to assess the role of NWUSC wildfires on
93 surface PM_{2.5} in the United States. The paper is organized as follows: We describe the data sets
94 used in this study followed by the GWR method. We then describe the results and discussion
95 followed by a summary with conclusions.

96

97 **2. Data**

98 A 17-day period (August 9th to August 25th) in 2018 (high fire activity) and 2011 (low fire
99 activity) was selected based on analysis of total fires (details in methodology section) to assess
100 surface PM_{2.5} (Table 1).

101 **2.1 Ground level PM_{2.5} observations:** Daily surface PM_{2.5} from the Environment Protection
102 Agency (EPA) are used in this study. These data are from Federal Reference Methods (FRM),
103 Federal Equivalent Methods (FEM), or other methods that are to be used in the National Ambient
104 Air Quality Standards (NAAQS) decisions. A total of 1003 monitoring sites in the US are included
105 in our study with 949 having valid observations in the study period in 2018, and a total of 873 sites
106 with 820 having valid observations in the study period in 2011. PM_{2.5} values less than 2 μgm^{-3}
107 are discarded since they are lower than the established detection limit (Hall et al., 2013).

108 **2.2 Satellite Data:** The MODIS mid visible AOD from the Multi-Angle Implementation of
109 Atmospheric Correction (MAIAC) product (MCD19A2 Version 6 data product) is used in this
110 study. We used MAIAC retrieved Terra and Aqua MODIS AOD product at 1 km pixel resolution
111 (Lyapustin et al., 2018). Different orbits are averaged to obtain mean daily values. Since thick
112 smoke plumes generated by the wildfires can be detected as cloud by a large chance, we preserve
113 possible cloud contaminated pixels to preserve the thick smoke pixels, and only AOD less than 0
114 will be discarded. Validation with AERONET studies show that 66% of the MAIAC AOD data

115 agree within $\pm 0.5 \sim \pm 0.1$ AOD (Lyapustin et al., 2018). Largely due to cloud cover, grid cells may
116 have limited number of AOD observations within a certain period. On average, cloud free AOD
117 data are available about 40% of the time during August 9th to August 25th in 2018 when fires were
118 active in the region bounded by 25~50°N, 65~125°W. [Smoke flag from the same product is used](#)
119 [as a predictor in estimating surface PM2.5. The smoke detection is performed using MODIS red,](#)
120 [blue and deep blue bands, and separate smoke pixels from dust and clouds based on absorption](#)
121 [parameter, size parameter and thermal threshold \(Lyapustin et al., 2018, 2012\). Smoke flag data](#)
122 [can provide the percentage of smoke pixel in each grid, which is related to smoke coverage.](#)

123 We also use the MODIS level-3 daily FRP (MCD14ML, fire radiative power) product
124 which combines Terra and Aqua fire products to assess wildfire activity. The fire radiative energy
125 indicates the rate of combustion and thus FRP can be used for characterizing active fires (Freeborn
126 et al, 2014). For purposes of the study we sum the FRP within every 2.3°×3.5° box to represent
127 the total fire activity in different locations.

128 **2.3 Meteorological data:** Meteorological information including boundary layer height (BLH), 2m
129 temperature (T2M), 10m wind speed (WS), surface relative humidity (RH) and surface pressure
130 (SP) are obtained from the European Centre for Medium-Range Weather Forecasts (ECMWF)
131 reanalysis (ERA5) product, with a spatial resolution of 0.25 degrees and temporal resolution of 1
132 hour and is matched temporally with the satellite overpass time. The BLH can provide information
133 of aerosol layer height as aerosols are often found to be well-mixed within the boundary layer
134 (Gupta and Christopher, 2009b). A higher RH will increase the hygroscopicity, change scattering
135 properties of certain aerosols and can lead to a higher AOD value (Zheng et al., 2017). In addition,
136 high surface temperatures can also accelerate the formation of secondary particles in the
137 atmosphere.

~~2.4 Land cover and population data: Land cover and population density is highly related to anthropogenic aerosol emissions, which also affects surface PM_{2.5}. Land cover information from the European Space Agency (ESA) with a spatial resolution of 300m and temporal resolution of one year (ESA, 2017) and population data from 'Gridded Population of the World', v4 (GPWv4) with a spatial resolution of 5 km are used as variables for the GWR method used in this study. The ESA land cover product uses global time series input datasets acquired by the Envisat Medium Resolution Imaging Spectrometer (MERIS) and from the SPOT Vegetation (SPOT VGT) sensors. The global land surface reflectance values are produced from the MERIS level 1 dataset, which along with SPOT VGT S1 (daily synthesis product) are used as input to the classification module and interprets into land cover classes. The population data uses results of the 2010 Population and Housing Census as input data.~~

3. Methodology

To assess the impact of NWUSC fires on PM_{2.5} in the United States, we first estimate the PM_{2.5} over the study region during a time period with high fire activity (2018). We then use the same method during a year with low fire activity (2011) to compare the differences between the two years. The two years are selected based on the total FRP in August calculated within Canada (49~60°N, 55~135°W) and Northwestern (NW) US (35~49°N, 105~125°W). Table 2 shows the total FRP in Canada and Northwestern US in August from 2010 to 2018. The total FRP in the two regions is lowest in 2011 and highest in 2018 during the 9 years, which provides the basis for the study. In order to create a 0.1° surface PM_{2.5}, the GWR model is used to estimate the relationships of PM_{2.5} and AOD. Detailed processing steps for GWR model are shown in Figure 1.

3.1 Data preprocessing: The first step is to resample all datasets to a uniform spatial resolution by creating a 0.1° resolution grid covering the Continental United States. During this process, we

161 collocate the PM_{2.5} data and average the values if there is more than one value in one grid. Then
162 the MAIAC AOD ~~and smoke flag, land cover and population data~~ are averaged into 0.1° grid cells.
163 Meteorological datasets are also resampled to the 0.1° grid cells by applying the inverse distance
164 method.

165 **3.2 Time selecting & averaging:** Next we select data where AOD and ground PM_{2.5} are both
166 available (AOD > 0 and PM_{2.5} > 2.0 $\mu\text{g m}^{-3}$) and average them for the study period. This is to
167 ensure that the AOD, PM_{2.5} and other variables match with each other, because PM_{2.5} is not a
168 continuous measurement for some sites and AOD have missing values due to cloud cover and
169 other reasons. Therefore, it is important to use data from days where both measurements are
170 available to avoid sampling biases.

171 **3.3 GWR model development and validation:** The Adaptive bandwidth selected by the Akaike's
172 Information Criterion (AIC) is used for the GWR model (Loader, 1999). For locations that already
173 have PM_{2.5} monitors, we calculate the mean AOD of a 0.5×0.5° box centered at the ground
174 location and estimate the GWR coefficients (β) for AOD and meteorological ~~land cover~~ variables
175 to estimate PM_{2.5}. The model structure can be expressed as:

$$176 \quad PM_{2.5i} = \beta_{0,i} + \beta_{1,i}AOD_i + \beta_{2,i}BLH_i + \beta_{3,i}T2M_i + \beta_{4,i}U10M_i + \beta_{5,i}RH_{sfci} + \beta_{6,i}SP_i + \beta_{7,i}LC_i \\ 177 \quad + \beta_{8,i}POP_i + \beta_{7,i}SF_i + \varepsilon_i$$

178 where $PM_{2.5i}$ ($\mu\text{g m}^{-3}$) is the selected ground-level PM_{2.5} concentration at location i ;
179 $\beta_{0,i}$ is the intercept at location i ; $\beta_{1,i} \sim \beta_{8,i}$ are the location-specific coefficients; AOD_i is the
180 resampled AOD selected from MAIAC daily AOD data at location i ;
181 $BLH_i, T2M_i, U10M_i, RH_{sfci}, SP_i$ are selected meteorological parameters (BLH, T2M, WS, RH and
182 PS) at location i ; ~~LC_i is the resampled land cover data at location i~~ ; POP_i ($\text{person}/\text{km}^2$) is the

183 ~~resampled population density at location i ; SF_i (%) is the resampled smoke flag data at location i~~
184 and ε_i is the error term at location i .

185 We perform the Leave One Out Cross Validation (LOOCV) to test the model predictive
186 performance (Kearns and Ron, 1999). Since the GWR model relies on adequate number of
187 observations, the prediction accuracy will be lower if we preserve too much data for validation.
188 Therefore, we choose the LOOCV method, which preserve only one data for validation at a time
189 and repeat the process until all the data are used. In addition, R^2 and RMSE are calculated for both
190 model fitting and model validation process to detect overfitting. Model overfitting will lead to low
191 predictability, which means it fits too close to the limited number of data to predict for other places
192 and will cause large bias.

193 **3.4 Model prediction:** While predicting the ground-level PM2.5 for unsampled locations, we
194 make use of the estimated parameters for sites within a 5° radius to generate new slopes for
195 independent variables based on the spatial weighting matrix (Brunsdon et al., 1996). The closer to
196 the predicted location, the closer to 1 the weighting factor will be, while the weighting factor for
197 sites further than the 5° in distance is zero. It is important to note that AOD and other independent
198 variables used for prediction in this step are averaged values for days that have valid AOD, which
199 is different from the data used in the fitting process since PM2.5 is not measured every day in all
200 locations.

201 **4. Results and Discussion**

202 We first discuss the surface PM2.5 for a few select locations that are impacted by fires
203 followed by the spatial distribution of MODIS AOD and the FRP for August 2018. We then assess
204 the spatial distribution of surface PM2.5 from the GWR method. The validation of the GWR

205 method is then discussed. To further demonstrate the impact of the NWUSC fires on PM2.5 air
206 quality in the United States, we show the spatial distribution of the difference between August
207 2018 and August 2011. We further quantify these results for ten US EPA regions.

208 **4.1 Descriptive statistics of satellite data and ground measurements**

209 The 2018 summertime Canadian wildfires started around the end of July in British
210 Columbia and continued until mid-September. The fires spread rapidly to the south of Canada
211 during August, causing high concentrations of smoke aerosols to drift down to the US and affecting
212 particulate matter air quality significantly. From late July to mid-September, wildfires in the
213 northwest US that burnt forest and grassland also affected air quality. Starting with the Cougar
214 Creek Fire, then Crescent Mountain and Gilbert Fires, different wildfires in in NWUSC caused
215 severe air pollution in various US cities. Figure 2a shows the rapid increase in PM2.5 of selected
216 US cities from July 1st to August 31st, due to the transport of smoke from these wildfires. For all
217 sites, July had low PM2.5 concentrations ($<10 \mu g m^{-3}$) and rapidly increases as fire activity
218 increases. Calculating only from the EPA ground observations, the mean PM2.5 of the 17 days for
219 the whole US is $13.7 \mu g m^{-3}$ and the mean PM2.5 for Washington (WA) is $40.6 \mu g m^{-3}$, which
220 indicates that the PM pollution is concentrated in the northwestern US for these days. This trend
221 is obvious when comparing the mean PM2.5 of all US stations (black line with no markers) and
222 the mean PM2.5 of all WA stations (grey line with no markers). Ground-level PM2.5 reaches its
223 peak between August 17th-21st and daily PM2.5 values during this time period far exceeds the 17-
224 day mean PM2.5. For example, mean PM2.5 in WA on August 20th is $86.75 \mu g m^{-3}$, which is
225 more than two times the 17-day average of this region. On August 19th, Omak which is located in
226 the foothills of the Okanogan Highlands in WA had PM2.5 values exceed $250 \mu g m^{-3}$. According
227 to a review of US wildfire caused PM2.5 exposures, 24-h mean PM2.5 concentrations from

228 wildfires ranged from 8.7 to 121 $\mu\text{g m}^{-3}$, with a 24 h maximum concentration of 1659 $\mu\text{g m}^{-3}$
229 (Navarro et al., 2018).

230 Table 3 shows relevant statistics of 15 states that have at least one daily record of non-
231 attainment of violating EPA standard ($>35 \mu\text{g m}^{-3}$ ~~(3)~~). From the frequency records of
232 violation non attainment in the 17-day period (last column), four states (Montana, Washington,
233 California and Idaho) were consistently affected by the wildfires, and large portion of ground
234 stations in these states were influenced by smoke aerosols, which represent that the pollution area
235 is large. Most of the neighboring states also suffered from short-term but broad air pollution (third
236 column). One thing nNoticeable from these records is that the total number of ground stations in
237 some of the highly affected states (such as Idaho) is not sufficient for capturing the smoke.
238 Although there are total 8 EPA stations in Idaho, only two of them have consistent observations
239 during the fire event; the other another two stations have no valid observations, and the
240 remaining other four stations have only 2~6 observations during the 17-day period. Limited valid
241 data along with unevenly distributed stations makes it hard to quantify smoke pollution in
242 Northwestern US during the fire event period. Therefore, we utilize bring in satellite data to enlarge
243 the spatial coverage and estimate pollution at a finer spatial resolution.

Formatted: Superscript

244 The spatial distribution of AOD shown in Figure 2b indicates that the smoke from Canada
245 is concentrated mostly in Northern US states such as WA, Oregon, Idaho, Montana, North Dakota
246 and Minnesota. The black arrow shows the mean 800hPa-level mean wind for 17 days, and the
247 length of the arrow represents the wind speed in ms^{-1} . Also shown in Figure 2b are wind speeds
248 close to the fire sources which are about 4~5 ms^{-1} , and according to the distances and wind
249 directions, it can take approximately 28~36 hours for the smoke to transport southeastward to
250 Washington state. Then the smoke continues to move east to other northern states such as Montana

251 and North Dakota. In addition, the grey circle represents the total fire radiative power (FRP) of
252 every 2.3×3.5-degree box. The reason for not choosing a smaller grid for the FRP is to not clutter
253 Figure 2b with information from small fires. The bigger the circle is, the stronger the fire is in that
254 grid and different sizes and its corresponding FRP values are shown in the lower right corner. It is
255 clear that the strongest fires in 2018 are located in the Tweedsmuir Provincial Park of British
256 Columbia in Canada (53.333N, 126.417W). The four separate lightning-caused wildfires burnt
257 nearly 301,549 hectares of the boreal forest. The total FRP of August 2018 in Canada is about
258 5362 (*1000 MW), while the total FRP of August 2011 in Canada is 48 (* 1000 MW). The 2011
259 fire was relatively weak compared to the 2018 Tweedsmuir Complex fire and we therefore use the
260 2011 air quality data as a baseline to quantify the 2018 fire influence on PM2.5 in the United
261 States.

262 **4.2 Model Fitting and validation**

263 The main goal for using GWR model is to help predict the spatial distribution of PM2.5
264 for places with no ground monitors while leveraging the satellite AOD and therefore it is important
265 to ensure that the model is robust. Figure 3a and 3b show the results for 2018 for GWR model
266 fitting for the entire US and the LOOCV models respectively. The color of the scatter plots
267 represents the probability density function (PDF) which calculates the relative likelihood that the
268 observed ground-level PM2.5 would equal the predicted value. The lighter the color is, the more
269 points are present, with a higher correlation. The model fitting process estimates the slope for each
270 variable and therefore the model can be fitted close to the observed PM2.5 and using this estimated
271 relationship we are able to assess surface PM2.5 using other parameters at locations where PM2.5
272 monitors are not available. The LOOCV process tests the model performance in predicting PM2.5.
273 If the results of LOOCV has a large bias from the model fitting, then the predictability of the model

274 is low. Higher R^2 difference and RMSE difference value indicate that the model is overfitting and
275 not suitable. The R^2 for the model fitting is 0.834, and the R^2 for the LOOCV is 0.797804; the
276 RMSE for the GWR model fitting is 3.464 $\mu g m^{-3}$, and for LOOCV the RMSE is 3.8477 $\mu g m^{-3}$.
277 There are minor differences between fitting R^2 and validation R^2 (0.0370-0.036) and between fitting
278 RMSE and validation RMSE (0.3760-0.37 $\mu g m^{-3}$) suggesting that the model is not over-fitting
279 and has stable predictability further indicating that the model can predict surface PM2.5 reliably.
280 In addition, we also performed a 20-fold cross validation by splitting the dataset into 20
281 consecutive folds, and each fold is used for validation while the 19 remaining folds form the
282 training set. The 20-fold cross validation has R^2 of 0.7456 and RMSE of 4.315 $\mu g m^{-3}$. The
283 increase/decrease in the cross validated R^2 and RMSE indicates the importance of sufficient data
284 used for fitting since a small decrease in the number of fitting data can reduce the model prediction
285 accuracy. Overall, the prediction error of the model is between 3~5 $\mu g m^{-3}$, which is a reasonable
286 error range for 17-day average prediction of PM2.5. For data greater than the EPA standard (35
287 $\mu g m^{-3}$), the model has a RMSE of 12.07 $\mu g m^{-3}$, which is a lot larger than the ~~whole model~~
288 RMSE when using the entire model. Therefore, the model has a tendency for underestimating
289 PM2.5 exceedances by around 12.07 $\mu g m^{-3}$. The larger the PM2.5 is, the greater the model
290 underestimates.

4.3 Predictors' influence during wildfires

292 Table 4 shows the mean and different region coefficients from the GWR model. Boxes are shown
293 in figure 4c in different colors: box1 (red) located in Washington state is nearby the fire sources; box2
294 (gold) located in Montana state is influenced from both neighboring states and remote smoke from Canada;
295 box3 (green) in Minnesota which is state located further from the fires and has minor increase in PM2.5 due
296 to remote smoke; box4 (black) in Pennsylvania state is the furthest from fires and has no obvious pollution

297 [increase. By comparing the coefficients in these boxes, predictors have different influence in different](#)
298 [locations. AOD has stronger influence on predicting PM2.5 closer to fire sources, but local emissions](#)
299 [become more dominant if the distances is large enough. The smoke flag is overall positive related to surface](#)
300 [PM2.5, while it could slightly negatively relate to PM2.5 around fire sources and northeastern coasts. PBL](#)
301 [is ~~are~~ negatively related to PM2.5 when the pollution is concentrated near the ~~around~~ surface \(fires or human-](#)
302 [made emissions\), while it appears to be positively related to PM2.5 at locations where the main pollution](#)
303 [source comes from remote wildfire smoke. Surface temperature have a relative stable positive correlation](#)
304 [with surface PM2.5, however, surface pressure and wind speeds ~~are~~ have negatively correlated ~~ion~~ with](#)
305 [PM2.5. Relative humidity, on the other hand, shows large variations on PM2.5 influence across the nation.](#)
306 [Around the wildfires where the RH is relative low, RH has a positive correlation with PM2.5 since](#)
307 [hygroscopicity would increase and leads to accumulation of PM2.5, but increasing RH can also decrease](#)
308 [PM2.5 concentration by overgrowing the PM2.5 particles to deposition at high RH environment](#) (Chen et
309 al., 2018).

Formatted: Font: 11 pt

310 **4.4.3 Predicted PM2.5 Distribution**

311 The mean PM2.5 distributions over the United States shown in Figure 4a is calculated by
312 averaging the surface PM2.5 data from ground monitors for the 17 days, which matches well with
313 the GWR model-predicted PM2.5 distributions shown in Figure 4b. The model estimation extends
314 the ground measurements and provide pollution assessments across the entire nation. Comparing
315 the AOD map (Figure 2b) with the PM2.5 estimations (Figure 4b), demonstrates the differences
316 between columnar and surface-level pollution. Differences between the AOD and PM2.5
317 distributions are due to various reasons including 1) Areas with high PM2.5 concentrations in
318 figure 4b correspond to low AOD values in figure 2b (Southern California, Utah, and southern
319 US); 2) and high AOD regions in figure 2b correspond to low PM2.5 concentrations in figure 4b
320 (Minnesota). The first situation usually occurs at the edge of polluted areas that are relative far

321 from the fire source, which is consistent with previous studies that reported smaller particles (<10
322 μg) are able to travel longer distances compared to large particles (>10 μg) (Gillies et al., 1996),
323 and that larger particles tend to settle closer to their source (Sapkota et al., 2005; Zhu et al., 2002).

324 We use the same method for August 9th to August 25th in 2011 that had low fire activity,
325 ensuring consistency for estimating coefficients for different variables for 2011. Figure 4c shows
326 the difference in spatial distribution of mean ground PM2.5 of the 17 days between 2018 and 2011.
327 High values of PM2.5 differences are in the Northwestern and central parts of the United States
328 with the Southern states having very little impact due to the fires. Of all the 48 states within the
329 study region, there are 29 states that have a higher PM2.5 value in 2018 than 2011, and 15 states
330 have 2018 PM2.5 value more than two times their 2011 value (shown in [table 3 figure 5](#)). The mean
331 PM2.5 for WA increases from 5.87 in 2011 to ~~47.4~~46.47 $\mu g m^{-3}$ in 2018, which is about 8 times
332 more than 2011 values. The PM2.5 values in Oregon increases from 4.97 (in 2011) to ~~33.3~~34
333 $\mu g m^{-3}$ in 2018, which is nearly seven times more than in 2011. For states from Montana to
334 Minnesota, the mean PM2.5 decreases from east to west, which reveals the path of smoke
335 transport. As shown in Figure 4c, there is a clear transport path of smoke from North Dakota all
336 the way to Texas. Along the path, smoke increases PM2.5 concentrations by ~~173~~168% in North
337 Dakota and ~~276.2~~% in Texas. Smoke aerosols transported over long distances contains fine
338 fraction PM which significantly affect the health of children, adults, and vulnerable groups.

339 Figure 5 shows the mean PM2.5 predicted from the GWR model of different EPA regions
340 for the 17 days in 2011 and 2018 (Hawaii and Alaska are not included). The most influenced region
341 is region 10, which has a 2018 mean PM2.5 value of ~~34.2~~34.27 $\mu g m^{-3}$ that is 6 times larger than the
342 values in 2011 (5.8 $\mu g m^{-3}$) values. The PM2.5 of region 8 and 9 have ~~2.7~~2.74 and ~~2.6~~2.65 times
343 increase in 2018 compared to 2011. Region 1~4 have lower PM2.5 in 2018 than 2011 possibly

344 due to Clean Air Act initiatives, absence of any major fire activities and further away for transported
345 aerosols. The emission reduction improves the US air quality and lower the PM_{2.5} every year, but
346 6 out of 10 EPA regions show significant increases in PM_{2.5} during the study period, which
347 indicates that the long-range transported wildfire smoke has become the new major pollutant in
348 the US.

349 **4.5.4 Estimation of Canadian fire pollution**

350 To evaluate the pollution caused only from Canadian fires, we did a rough assessment
351 according to the total FRP and PM_{2.5} values. There are three states in the US have wildfires during
352 the study period: California, Washington and Oregon, and they have total FRP of 1186, 518 and
353 439 (*1000 MW) respectively. Assuming that California was only influenced by the local fires,
354 then fires of 1186 (*1000 MW) cause $13 \mu\text{g m}^{-3}$ increase in PM_{2.5}. Accordingly, wildfires in
355 Washington and Oregon State will cause 6 and $5 \mu\text{g m}^{-3}$ increase in state mean PM_{2.5}. Therefore,
356 Canadian fires caused PM_{2.5} increase in Washington and Oregon is about 35 and $23 \mu\text{g m}^{-3}$.
357 Since the FRP of Canadian wildfires are approximately 5 times larger than that of the California
358 fires, which is the strongest fire in US, we assume the pollution affecting the states located in the
359 downwind directions other than the three states are mainly coming from Canadian wildfires. States
360 with no local fires such as Montana, North Dakota, South Dakota and Minnesota have PM_{2.5}
361 increase of 18.31, 12.8, 10.4 and $10.13 \mu\text{g m}^{-3}$. The decrease of these numbers reveal that the
362 smoke is transport in a SE direction. This influence of Canadian wildfires on US air quality is only
363 a rough quantity estimation, thus additional work is needed for understand long-range transport
364 smoke pollution and its impact on public health. One way to do this would be assessing the
365 difference of pollution by turning on and off US fires in chemistry models.

366 **4.6.4 Model uncertainties and limitations**

367 There are various sources of uncertainties and limitations for studies that use satellite data
368 to estimate surface PM_{2.5} concentrations. Since wildfires develop quickly it is important to have
369 continuous observations to capture the rapid changes. This study uses polar orbiting high-quality
370 satellite aerosol products, but the temporal evolution can only be estimated by geostationary data
371 sets. Although satellite observations have excellent spatial coverage, missing data due to cloud
372 cover is a limitation. As discussed in the paper, the prediction error (RMSE) of the model is
373 between 3~5 $\mu\text{g m}^{-3}$. The GWR model is largely influenced by the distribution of ground stations,
374 and the prediction error will be different in different places due to unevenly distributed PM_{2.5}
375 stations. For locations that have a dense ground-monitoring distribution, the prediction error will
376 be low, while the prediction error will be relative larger at other places with sparse surface stations.
377 Although there are obvious limitations, complementing surface data with satellite products and
378 meteorological and other ancillary information in a statistical model like the GWR has provided
379 robust results for estimating surface PM_{2.5} from wildfires. We also note that we did not consider
380 some variables used in other studies such as NDVI, forest cover, vegetation type, industrial
381 density, visibility and chemical constituents of smoke particles (Donkelaar et al., 2015; Hu et al.,
382 2013; You et al., 2015; Zou et al., 2016). ~~While Land cover and land use information can improve
383 PM_{2.5} estimation predictability, redundant information such as NDVI can cause overfitting of
384 models. Therefore, in order to control the number of predictors used in the GWR model, we use
385 only one piece of land cover information. However, which of the land cover and land use
386 information performs better in predicting surface PM_{2.5} is still to be assessed in the future.~~
387 Visibility mentioned in some studies may improve the model performance, but unlike AOD, it has
388 limited measurement across the nation, which will restrict the applicability of training data.

389 [One limitation of this study is that analysis based on 17-day mean values cannot capture](#)
390 [daily pollution variations, which is also very important for pollution estimation during rapid-](#)
391 [changing wildfire events. To extend this analysis to daily estimation, the cloud contaminations of](#)
392 [satellite observations become a major problem. Therefore, future work is needed using chemistry](#)
393 [transport models and other data to fill in the gaps on missing AOD data due to cloud coverage.](#)

394 5. Summary and Conclusions

395 We estimate the surface mean PM_{2.5} for 17 days in August for a high fire active year
396 (2018) and compare that with a low fire activity year using the Geographically Weighted
397 Regression (GWR) method to assess the increase in PM_{2.5} in the United States due to smoke
398 transported from fires. The difference in PM_{2.5} between the two years indicates that more than
399 half of the US states (29 states) are influenced by the NWUSC wildfires, and half of the affected
400 states have 17-day mean PM_{2.5} increases larger than 100% of the baseline value. The peak PM_{2.5}
401 during the wildfires can be much larger than the 17-day average and can affect vulnerable
402 populations susceptible to air pollution. Some of the most affected states are in Washington,
403 California, Wisconsin, Colorado and Oregon, all of which have populations greater than 4 million.
404 According to CDC (Centers for Disease Control and Prevention), 8% of the population have
405 asthma (CDC, 2011). Therefore, for asthma alone, there are about 3 million people facing
406 significant health issue due to the long-range transport smoke in these states.

407 For states that show decrease in PM_{2.5} due to the Clean Air Act, the mean decrease is
408 about 16% of the baseline after 7 years. This is consistent with EPA's report that there is a 23%
409 decrease of PM_{2.5} in national average from 2010 to 2019 (U.S. Environmental Protection Agency,
410 2019). Comparing with the dramatic increase (132%) caused by wildfires, pollution from the fires
411 is counteracting our effort on emission controls. Although wildfires are often episodic and short-

412 term, high frequency of fire occurrence and increasing longer durations of summertime wildfires
413 in recent years has made them now a long-term influence on public lives. Our results show a
414 significant increase of pollution in a short time period in most of the US states due to the NWUSC
415 wildfires, which affects millions of people. With wildfires becoming more frequent during recent
416 years, more effort is needed to predict and warn the public about the long-range transported smoke
417 from wildfires.

418 ~~This study is novel in: 1) applying PM2.5 estimation methods on wildfire events and~~
419 ~~calculate the prediction error at high pollution concentration condition; 2) analyzing predictors'~~
420 ~~different influences in estimating PM2.5 under various conditions; 3) quantify the air pollution~~
421 ~~from fires by states and EPA regions.~~

Formatted: Indent: First line: 0.5"

422 Acknowledgements.

423 Pawan Gupta was supported by a NASA Grant. MODIS data were acquired from the Goddard
424 DAAC. We thank all the data providers for making this research possible.

425 References

426
427 Apte, J.S., Brauer, M., Cohen, A.J., Ezzati, M., Pope, C.A., 2018. Ambient PM2.5 Reduces

428 Global and Regional Life Expectancy. Environ. Sci. Technol. Lett. 5, 546–551.

429 <https://doi.org/10.1021/acs.estlett.8b00360>

430 Brunsdon, C., Fotheringham, A.S., Charlton, M.E., 1996. Geographically Weighted Regression:

431 A Method for Exploring Spatial Nonstationarity. Geogr. Anal. 28, 281–298.

432 <https://doi.org/https://doi.org/10.1111/j.1538-4632.1996.tb00936.x>

Formatted: Justified

Xue, Gupta, Christopher, submitted to Remote Sensing of Environment

- 433 Calkin, D.E., Thompson, M.P., Finney, M.A., 2015. Negative consequences of positive
434 feedbacks in us wildfire management. *For. Ecosyst.* 2, 1–10.
435 <https://doi.org/10.1186/s40663-015-0033-8>
- 436 Cascio, W.E., 2018. Wildland Fire Smoke and Human Health. *Sci. Total Environ.* 624, 586–595.
437 <https://doi.org/10.1016/j.scitotenv.2017.12.086>.
- 438 CDC, 2011. Asthma in the US. *CDC Vital Signs* 1–4.
- 439 Chen, Z., Xie, X., Cai, J., Chen, D., Gao, B., He, B., Cheng, N., Xu, B., 2018. Understanding
440 meteorological influences on PM_{2.5} concentrations across China: A temporal and spatial
441 perspective. *Atmos. Chem. Phys.* 18, 5343–5358. <https://doi.org/10.5194/acp-18-5343-2018>
- 442 Chu, Y., Liu, Y., Li, X., Liu, Z., Lu, H., Lu, Y., Mao, Z., Chen, X., Li, N., Ren, M., Liu, F., Tian,
443 L., Zhu, Z., Xiang, H., 2016. A review on predicting ground PM_{2.5} concentration using
444 satellite aerosol optical depth. *Atmosphere (Basel)*. 7, 129.
445 <https://doi.org/10.3390/atmos7100129>
- 446 Coogan, S.C.P., Robinne, F.N., Jain, P., Flannigan, M.D., 2019. Scientists’ warning on wildfire
447 — a canadian perspective. *Can. J. For. Res.* 49, 1015–1023. [https://doi.org/10.1139/cjfr-](https://doi.org/10.1139/cjfr-2019-0094)
448 [2019-0094](https://doi.org/10.1139/cjfr-2019-0094)
- 449 Donkelaar, A. Van, Martin, R. V., Li, C., Burnett, R.T., 2019. Regional Estimates of Chemical
450 Composition of Fine Particulate Matter Using a Combined Geoscience-Statistical Method
451 with Information from Satellites, Models, and Monitors. *Environ. Sci. Technol.* 53, 2595–
452 2611. <https://doi.org/10.1021/acs.est.8b06392>
- 453 Donkelaar, A. Van, Martin, R. V., Park, R.J., 2006. Estimating ground-level PM_{2.5} using

Xue, Gupta, Christopher, submitted to Remote Sensing of Environment

- 454 aerosol optical depth determined from satellite remote sensing. *J. Geophys. Res. Atmos.*
455 111. <https://doi.org/10.1029/2005JD006996>
- 456 Donkelaar, A. Van, Martin, R. V, Spurr, R.J.D., Burnett, R.T., 2015. High-Resolution Satellite-
457 Derived PM_{2.5} from Optimal Estimation and Geographically Weighted Regression over
458 North America. *Environ. Sci. Technol.* 49, 10482–10491.
459 <https://doi.org/10.1021/acs.est.5b02076>
- 460 Dreessen, J., Sullivan, J., Delgado, R., 2016. Observations and impacts of transported Canadian
461 wildfire smoke on ozone and aerosol air quality in the Maryland region on June 9–12, 2015.
462 *J. Air Waste Manag. Assoc.* 66, 842–862. <https://doi.org/10.1080/10962247.2016.1161674>
- 463 Fotheringham, A.S., Charlton, M.E., Brunson, C., 1998. Geographically weighted regression: a
464 natural evolution of the expansion method for spatial data analysis. *Environ. Plan. A* 30,
465 1905–1927.
- 466 Fotheringham, S.A., Brunson, C., Charlton, M., 2003. Geographically Weighted Regression :
467 The Analysis of Spatially Varying Relationships, John Wiley and Sons.
- 468 Freeborn, P.H., Wooster, M.J., Roy, D.P., Cochrane, M.A., 2014. Quantification of MODIS fire
469 radiative power (FRP) measurement uncertainty for use in satellite-based active fire
470 characterization and biomass burning estimation. *Geophys. Res. Lett.* 41, 1988–1994.
471 <https://doi.org/10.1002/2013GL059086>.
- 472 Goldberg, D.L., Gupta, P., Wang, K., Jena, C., Zhang, Y., Lu, Z., Streets, D.G., 2019. Using gap-
473 filled MAIAC AOD and WRF-Chem to estimate daily PM_{2.5} concentrations at 1 km
474 resolution in the Eastern United States. *Atmos. Environ.* 199, 443–452.
475 <https://doi.org/10.1016/j.atmosenv.2018.11.049>

Xue, Gupta, Christopher, submitted to Remote Sensing of Environment

- 476 Gu, Y., 2019. Estimating PM_{2.5} Concentrations Using 3 km MODIS AOD Products : A Case
477 Study in British Columbia , Canada. University of Waterloo.
- 478 Guo, B., Wang, X., Pei, L., Su, Y., Zhang, D., Wang, Y., 2021. Identifying the spatiotemporal
479 dynamic of PM_{2.5} concentrations at multiple scales using geographically and temporally
480 weighted regression model across China during 2015–2018. *Sci. Total Environ.* 751.
481 <https://doi.org/10.1016/j.scitotenv.2020.141765>
- 482 Gupta, P., Christopher, S.A., 2009a. Particulate matter air quality assessment using integrated
483 surface, satellite, and meteorological products: 2. A neural network approach. *J. Geophys.*
484 *Res. Atmos.* 114, 1–14. <https://doi.org/10.1029/2008JD011497>
- 485 Gupta, P., Christopher, S.A., 2009b. Particulate matter air quality assessment using integrated
486 surface , satellite , and meteorological products : Multiple regression approach. *J. Geophys.*
487 *Res. Atmos.* 114, 1–13. <https://doi.org/10.1029/2008JD011496>
- 488 Hall, E.S., Kaushik, S.M., Vanderpool, R.W., Duvall, R.M., Beaver, M.R., Long, R.W.,
489 Solomon, P.A., 2013. Intergrating Sensor Monitoring Technology into Current Air
490 Pollution Regulatory Support Paradigm: Practical Considerations. *Am. J. Environ. Eng* 4,
491 147–154. <https://doi.org/10.5923/j.ajee.20140406.02>
- 492 Hessburg, P.F., Churchill, D.J., Larson, A.J., Haugo, R.D., Miller, C., Spies, T.A., North, M.P.,
493 Povak, N.A., Belote, R.T., Singleton, P.H., Gaines, W.L., Keane, R.E., Aplet, G.H.,
494 Stephens, S.L., Morgan, P., Bisson, P.A., Rieman, B.E., Salter, R.B., Reeves, G.H., 2015.
495 Restoring fire-prone Inland Pacific landscapes: seven core principles. *Landsc. Ecol.* 30,
496 1805–1835. <https://doi.org/10.1007/s10980-015-0218-0>
- 497 Hoff, R.M., Christopher, S.A., 2009. Remote Sensing of Particulate Pollution from Space : Have

Xue, Gupta, Christopher, submitted to Remote Sensing of Environment

- 498 We Reached the Promised Land ? J. Air Waste Manage. Assoc. 59, 645–675.
499 <https://doi.org/10.3155/1047-3289.59.6.645>
- 500 Hu, X., Waller, L.A., Al-Hamdan, M.Z., Crosson, W.L., Estes, M.G., Estes, S.M., Quattrochi,
501 D.A., Sarnat, J.A., Liu, Y., 2013. Estimating ground-level PM_{2.5} concentrations in the
502 southeastern U.S. using geographically weighted regression. Environ. Res. 121, 1–10.
503 <https://doi.org/10.1016/j.envres.2012.11.003>
- 504 Hu, Z., 2009. Spatial analysis of MODIS aerosol optical depth, PM_{2.5}, and chronic coronary
505 heart disease. Int. J. Health Geogr. 8, 1–10. <https://doi.org/10.1186/1476-072X-8-27>
- 506 Hubbell, B.J., Crume, R. V., Evarts, D.M., Cohen, J.M., 2010. Policy Monitor: Regulation and
507 progress under the 1990 Clean Air Act Amendments. Rev. Environ. Econ. Policy 4, 122–
508 138. <https://doi.org/10.1093/reep/rep019>
- 509 Hystad, P., Demers, P.A., Johnson, K.C., Brook, J., Van Donkelaar, A., Lamsal, L., Martin, R.,
510 Brauer, M., 2012. Spatiotemporal air pollution exposure assessment for a Canadian
511 population-based lung cancer case-control study. Environ. Heal. A Glob. Access Sci.
512 Source 11, 1–22. <https://doi.org/10.1186/1476-069X-11-22>
- 513 J.A.Gillies, W.G.Nickling, G.H.Mctainsh, 1996. Dust concentration s and particle-size
514 characteristics of an intense dust haze event: inland delta region. Atmos. Environ. 30, 1081–
515 1090.
- 516 Kearns, M., Ron, D., 1999. Algorithmic stability and sanity-check bounds for leave-one-out
517 cross-validation. Neural Comput. 11, 1427–1453.
518 <https://doi.org/10.1162/089976699300016304>

- 519 Kollanus, V., Tiittanen, P., Niemi, J. V., Lanki, T., 2016. Effects of long-range transported air
520 pollution from vegetation fires on daily mortality and hospital admissions in the Helsinki
521 metropolitan area, Finland. *Environ. Res.* 151, 351–358.
522 <https://doi.org/10.1016/j.envres.2016.08.003>
- 523 Liu, Y., Sarnat, J.A., Kilaru, V., Jacob, D.J., Koutrakis, P., 2005. Estimating ground-level PM2.5
524 in the eastern United States using satellite remote sensing. *Environ. Sci. Technol.* 39, 3269–
525 3278. <https://doi.org/10.1021/es049352m>
- 526 Loader, C.R., 1999. BANDWIDTH SELECTION: CLASSICAL OR PLUG-IN? *Ann. Stat.* 27,
527 415–438.
- 528 Lyapustin, A., Korkin, S., Wang, Y., Quayle, B., Laszlo, I., 2012. Discrimination of biomass
529 burning smoke and clouds in MAIAC algorithm. *Atmos. Chem. Phys.* 12, 9679–9686.
530 <https://doi.org/10.5194/acp-12-9679-2012>
- 531 Lyapustin, A., Wang, Y., Korkin, S., Huang, D., 2018. MODIS Collection 6 MAIAC Algorithm.
532 *Atmos. Meas. Tech.* 11, 5741–5765. <https://doi.org/10.5194/amt-2018-141>
- 533 Ma, Z., Hu, X., Huang, L., Bi, J., Liu, Y., 2014. Estimating ground-level PM2.5 in china using
534 satellite remote sensing. *Environ. Sci. Technol.* 48, 7436–7444.
535 <https://doi.org/10.1021/es5009399>
- 536 Meixner, T., Wohlgemuth, P., 2004. Wildfire Impacts on Water Quality. *J. Wildl. Fire* 13, 27–
537 35.
- 538 Melillo, J.M., Richmond, T., Yohe, G.W., 2014. Climate Change Impacts in the United States.
539 *Third Natl. Clim. Assess.* 52. <https://doi.org/10.7930/J0Z31WJ2>.

Xue, Gupta, Christopher, submitted to Remote Sensing of Environment

- 540 Miller, D.J., Sun, K., Zondlo, M.A., Kanter, D., Dubovik, O., Welton, E.J., Winker, D.M.,
541 Ginoux, P., 2011. Assessing boreal forest fire smoke aerosol impacts on U.S. air quality: A
542 case study using multiple data sets. *J. Geophys. Res. Atmos.* 116.
543 <https://doi.org/10.1029/2011JD016170>
- 544 Mirzaei, M., Bertazzon, S., Couloigner, I., 2018. Modeling Wildfire Smoke Pollution by
545 Integrating Land Use Regression and Remote Sensing Data : Regional Multi-Temporal
546 Estimates for Public Health and Exposure Models. *Atmosphere (Basel)*. 9, 335.
547 <https://doi.org/10.3390/atmos9090335>
- 548 Munoz-alpizar, R., Pavlovic, R., Moran, M.D., Chen, J., Gravel, S., Henderson, S.B., Sylvain,
549 M., Racine, J., Duhamel, A., Gilbert, S., Beaulieu, P., Landry, H., Davignon, D., Cousineau,
550 S., Bouchet, V., 2017. Multi-Year (2013–2016) PM_{2.5} Wildfire Pollution Exposure over
551 North America as Determined from Operational Air Quality Forecasts. *Atmosphere (Basel)*.
552 8, 179. <https://doi.org/10.3390/atmos8090179>
- 553 Navarro, K.M., Schweizer, D., Balmes, J.R., Cisneros, R., 2018. A review of community smoke
554 exposure from wildfire compared to prescribed fire in the United States. *Atmosphere*
555 *(Basel)*. 9, 1–11. <https://doi.org/10.3390/atmos9050185>
- 556 Samet, J.M., 2011. The clean air act and health - A clearer view from 2011. *N. Engl. J. Med.*
557 365, 198–201. <https://doi.org/10.1056/NEJMp1103332>
- 558 Sapkota, A., Symons, J.M., Kleissl, J., Wang, L., Parlange, M.B., Ondov, J., Breyse, P.N.,
559 Diette, G.B., Eggleston, P.A., Buckley, T.J., 2005. Impact of the 2002 Canadian forest fires
560 on particulate matter air quality in Baltimore City. *Environ. Sci. Technol.* 39, 24–32.
561 <https://doi.org/10.1021/es035311z>

Xue, Gupta, Christopher, submitted to Remote Sensing of Environment

- 562 Stephens, S.L., 2005. Forest fire causes and extent on United States Forest Service lands. *Int. J.*
563 *Wildl. Fire* 14, 213–222. <https://doi.org/10.1071/WF04006>
- 564 U.S. Environmental Protection Agency, 2019. Particulate Matter (PM2.5) Trends.
- 565 You, W., Zang, Z., Pan, X., Zhang, L., Chen, D., 2015. Estimating PM2.5 in Xi'an, China using
566 aerosol optical depth: A comparison between the MODIS and MISR retrieval models. *Sci.*
567 *Total Environ.* 505, 1156–1165. <https://doi.org/10.1016/j.scitotenv.2014.11.024>
- 568 You, W., Zang, Z., Zhang, L., Li, Y., Pan, X., Wang, W., 2016. National-scale estimates of
569 ground-level PM2.5 concentration in China using geographically weighted regression based
570 on 3 km resolution MODIS AOD. *Remote Sens.* 8. <https://doi.org/10.3390/rs8030184>
- 571 Zhang, H., Hoff, R.M., Engel-Cox, J.A., 2009. The relation between moderate resolution
572 imaging spectroradiometer (MODIS) aerosol optical depth and PM2.5 over the United
573 States: A geographical comparison by U.S. Environmental Protection Agency regions. *J.*
574 *Air Waste Manag. Assoc.* 59, 1358–1369. <https://doi.org/10.3155/1047-3289.59.11.1358>
- 575 Zheng, C., Zhao, C., Zhu, Y., Wang, Y., Shi, X., Wu, X., Chen, T., Wu, F., Qiu, Y., 2017.
576 Analysis of influential factors for the relationship between PM2.5 and AOD in Beijing.
577 *Atmos. Chem. Phys.* 17, 13473–13489. <https://doi.org/10.5194/acp-17-13473-2017>
- 578 Zhu, Y., Hinds, W.C., Kim, S., Sioutas, C., 2002. Concentration and size distribution of ultrafine
579 particles near a major highway. *J. Air Waste Manag. Assoc.* 52, 1032–1042.
580 <https://doi.org/10.1080/10473289.2002.10470842>
- 581 Zou, B., Pu, Q., Bilal, M., Weng, Q., Zhai, L., Nichol, J.E., 2016. High-resolution Satellite
582 Mapping of Fine Particulates Based on Geographically Weighted Regression. *Ieee Geosci.*

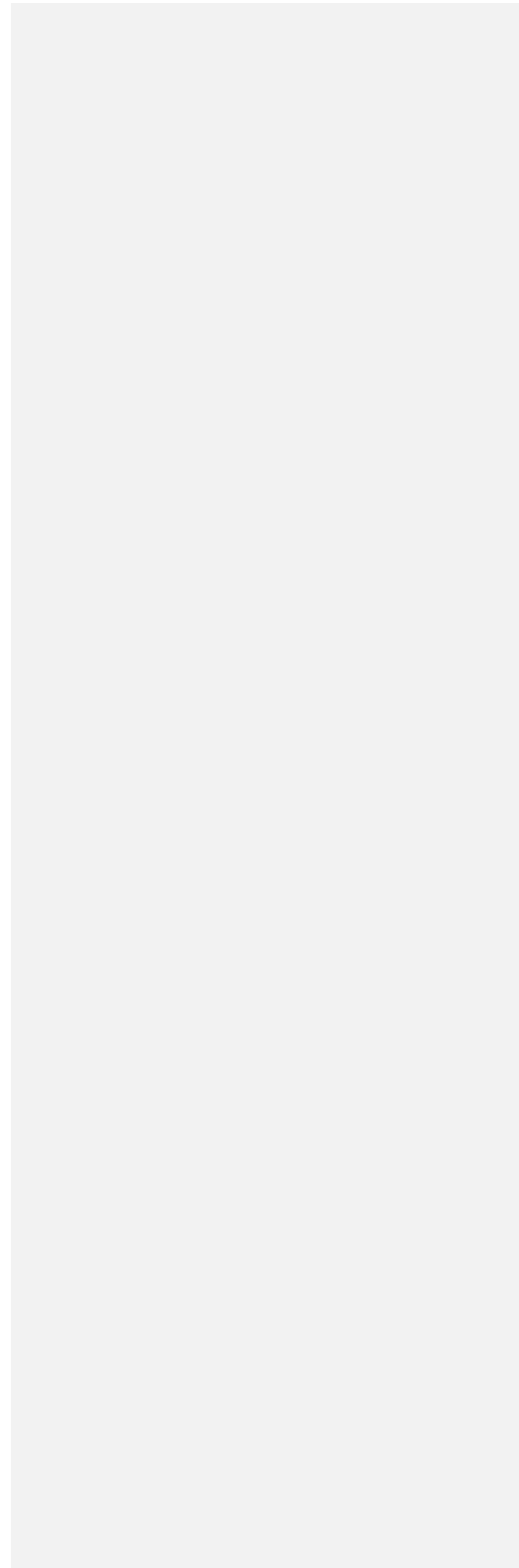
Xue, Gupta, Christopher, submitted to Remote Sensing of Environment

583 Remote Sens. Lett. 13, 495–499.

584

585

586



587 Table 1. Datasets used in the study with sources.

588

	Data /Model	Sensor	Spatial Resolution	Temporal Resolution	Accuracy
1	Surface PM2.5	TEOM	Point data	daily	±5~10%
2	Mid visible aerosol optical depth (AOD)	MAIAC_ MODIS	1km	daily	66% compared to AERONET
3	Fire Radiative Power (FRP)	Terra/Aqua- MODIS	1km	daily	± 7%
4	ECMWF (Meteorological variables)		0.25 degree	hourly	
5	Land-cover	MERIS SR	300m	Annual	

Formatted Table

589 1) <https://www.epa.gov/outdoor-air-quality-data>

590 2) <https://earthdata.nasa.gov/>

591 3) <https://earthdata.nasa.gov/>

592 4) <https://www.ecmwf.int/en/forecasts>

593 5) <https://www.esa-landcover-cci.org>

594 6) <https://sedac.ciesin.columbia.edu/data/collection/gpw-v4>

595

596

597

598 Table 2. Total FRP in Canada and Northwestern US in August of Different Years (unit: 10⁴

599 MW)

Year	2010	2011	2012	2013	2014	2015	2016	2017	2018
CA	148.24	4.84	19.93	70.54	107.78	10.39	4.6	307.3	542.99
NW US	16.41	42.84	320.39	192.06	67.01	339.58	112.9	195.64	296.91

600

601 [Table 3. statistics of 15 states that violate EPA standards \(35 μg m⁻³\) during the 17-day wildfire](#)
 602 [period](#)

State	number of site violate standard	number of site in the state	Percentage of site violate standard (%)	number of days violate standard
Montana	14	15	93.34	16
Washington	18	20	90	16
Oregon	12	14	85.71	5
North Dakota	7	11	63.63	4
Idaho	5	8	62.5	8
Colorado	11	21	52.38	2
South Dakota	5	10	50	1
California	57	119	47.9	14
Utah	7	15	46.67	4
Nevada	4	13	30.77	1
Wyoming	7	24	29.2	2
Minnesota	4	26	15.4	2
Texas	3	37	8.1	1
Louisiana	1	14	7.1	1
Arizona	1	20	5	1

Formatted Table

603

604 [Table 4. Coefficients of different predictors](#)

	AOD	Smoke flag	PBL	T2M	RH	U	SP
box1(red)	92.01	-0.13	-1.5	0.2	-0.01	-1.6	-0.037
box2(gold)	63.97	0.002	-2.86	0.09	-0.11	-1.5	-0.02
box3(green)	5.9	0.044	0.3	0.16	0.017	-0.2	-0.015
box4(black)	6.72	-0.02	-1.3	0.28	-0.03	0.13	-0.007
mean	28.1	0.02	-0.89	0.06	-0.19	-0.67	-0.002

Formatted Table

605

Formatted: Line spacing: single

606

Table 3. Mean PM2.5 from August 9th to August 25th in 2018 and 2011 of different states

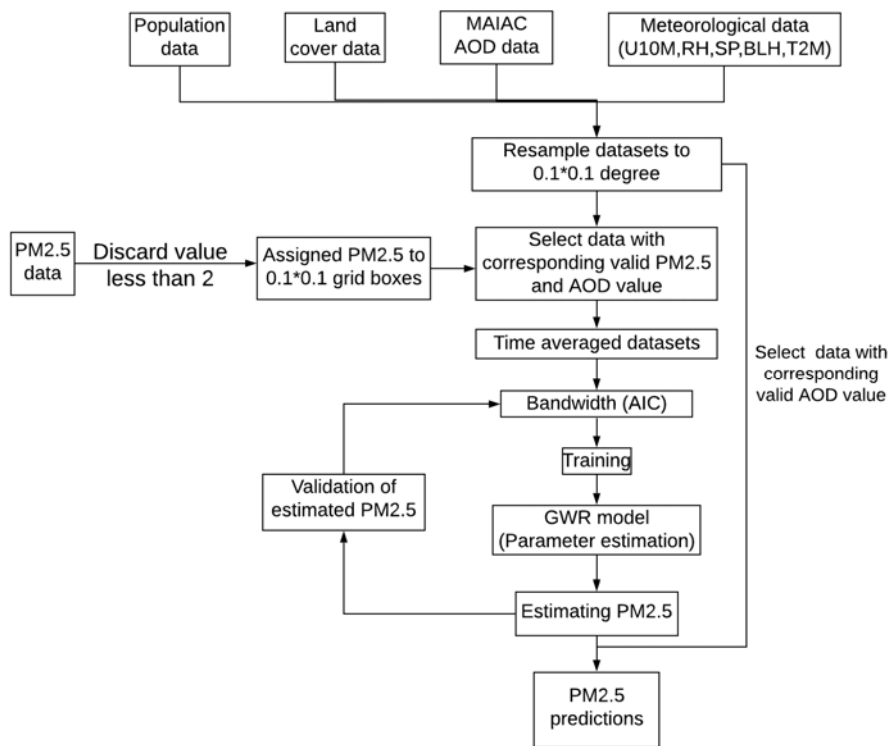
State	2018	2011
WA	47.0	5.874
OR	33.10	4.97
ID	26.26	6.79
MT	25.86	7.55
CA	21.22	7.66
ND	20.20	7.41
NV	17.92	5.51
SD	17.72	7.31
MN	16.41	6.27
WY	15.71	6.59
NE	15.69	6.81
UT	14.87	6.51
IA	14.73	7.87
KS	14.13	6.84
AR	13.92	11.59
WI	13.70	6.26
OK	13.53	9.26
MO	13.25	9.64
LA	13.24	13.07
IL	12.98	11.36
MS	12.86	13.67
CO	12.31	6.07
MI	11.97	6.82
TX	11.70	9.27
TN	11.66	14.39
AL	11.65	14.97
IN	11.50	12.51
KY	11.02	13.19
DC	10.65	13.16
NJ	10.56	9.76
DE	10.37	11.16
GA	10.22	14.02
CT	10.20	9.74
OH	10.14	11.84
FL	10.13	10.68
MD	10.07	12.59
NM	9.842	6.03
SC	9.829	12.66
PA	9.75	12.64
NC	9.67	12.44

Xue, Gupta, Christopher, submitted to Remote Sensing of Environment

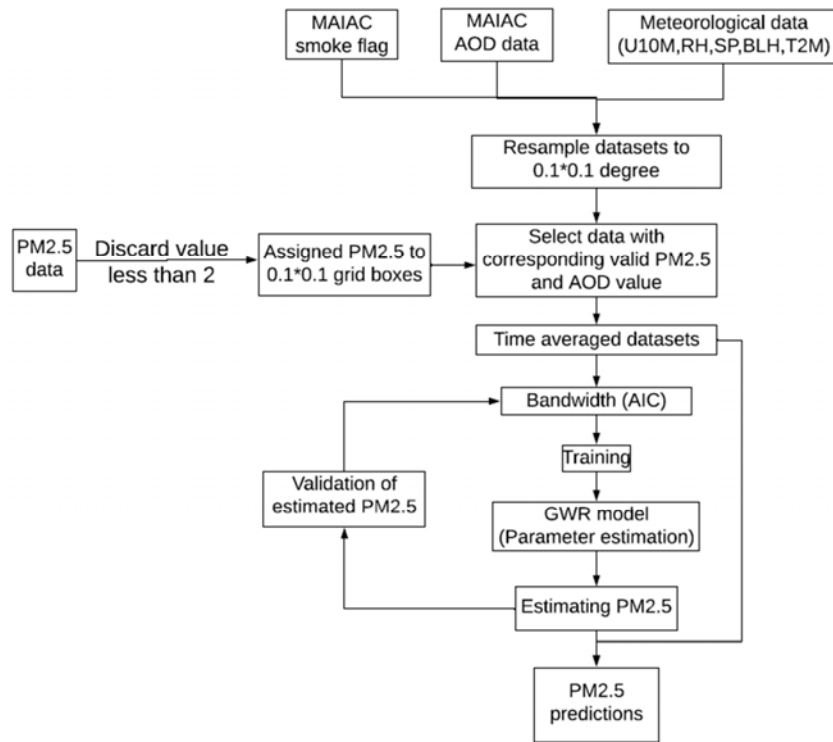
RI	9.633	8.602
MA	9.56	9.413
VA	9.38	13.74
NY	9.33	9.731
WV	9.28	13.58
NH	9.11	9.33
AZ	9.08	7.00
VT	8.96	9.34
ME	7.972	10.52

607
608
609
610
611
612
613

Formatted: Left



614



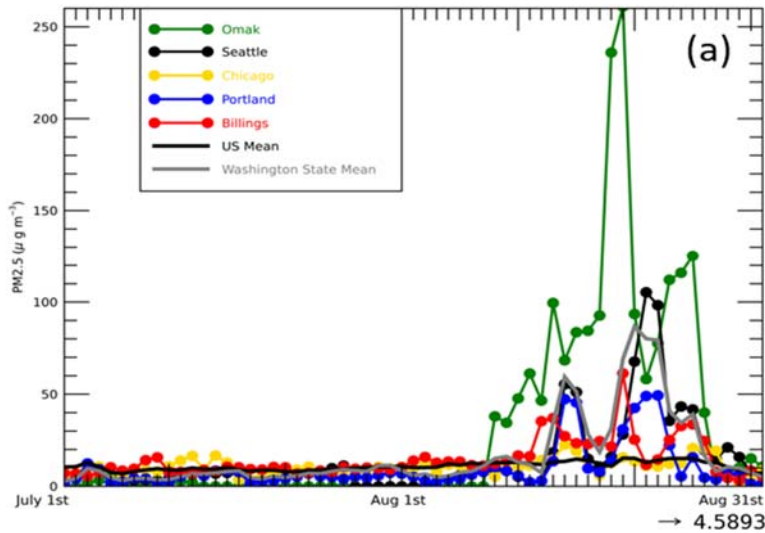
615

616 Figure 1. Flow chart for the Geographically Weighted Regression model used. All satellite,

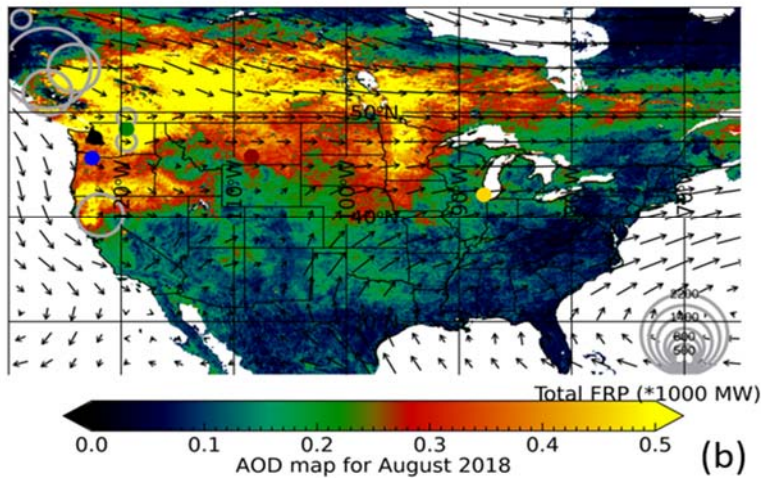
617 ground, meteorological data are gridded to 0.1 by 0.1 degrees.

618

619

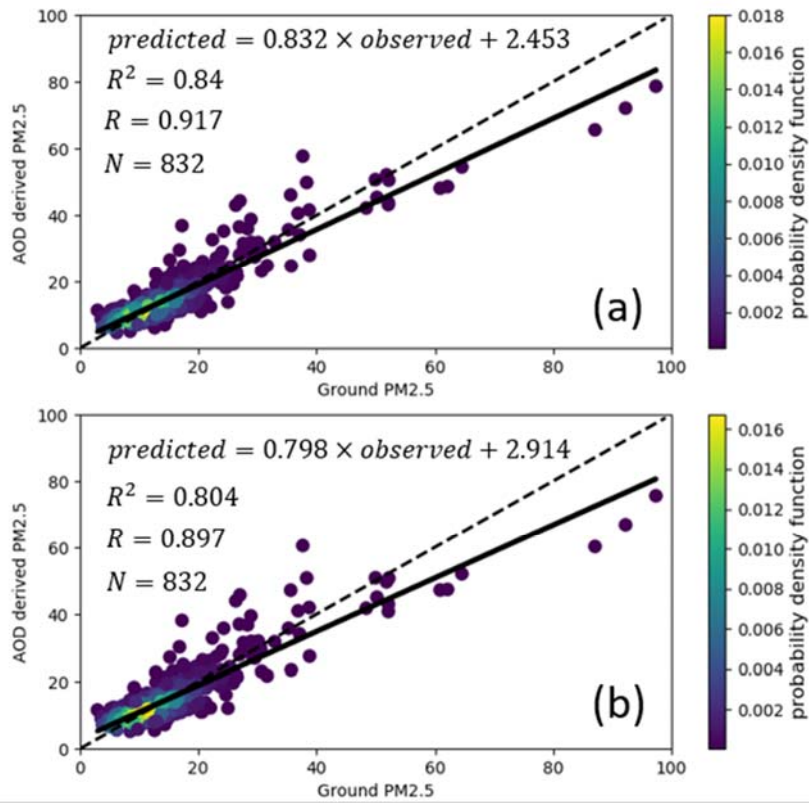


620

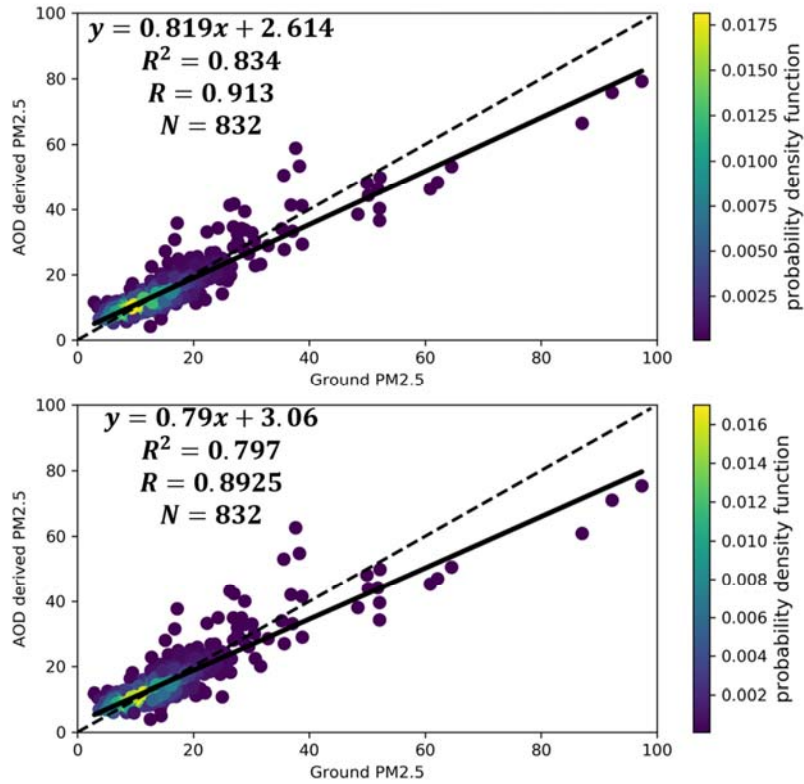


621

622 Figure 2. (a) Variations of EPA ground observed PM_{2.5} in different cities from July to August
623 2018 (Omak-Washington, Seattle-Washington, Chicago-Illinois, Portland-Oregon, Billings-
624 Montana). Black line without markers shows the mean variation of the whole US stations and the
625 grey line without markers shows the mean variation of stations in Washington state. (b) Mean
626 MAIAC satellite AOD distribution from August 9th to August 25th, 2018. AOD values equal or
627 larger than 0.5 are shown as the same color (yellow). Also shown are circles with Fire Radiative
628 Power (FRP). Black arrow shows the wind direction and the length of it represents the wind
629 speed. The round spots of different colors on the map show the locations of the five selected
630 cities (green-Omak, black-Seattle, yellow-Chicago, blue-Portland, red-Billings).



631



632

633 Figure 3. Results of model fitting and cross validation for GWR model for the entire US region
634 averaged from August 9th to August 25th, 2018. (a) GWR model fitting results (b) GWR model
635 LOOCV results. The dash line is the 1:1 line as reference and the black line shows the regression
636 line. The color of the scatter plots represents the probability density function which provides a
637 relative likelihood that the value of the random variable would equal a certain sample.

638

639

640

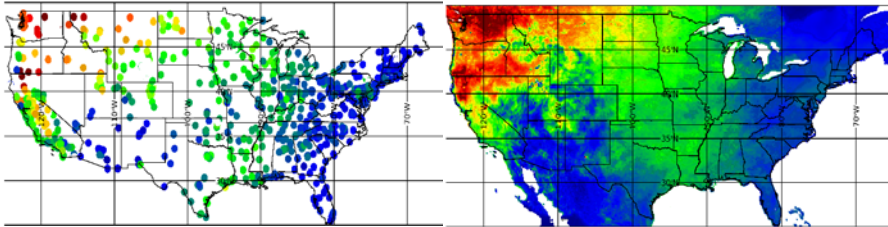
641

642

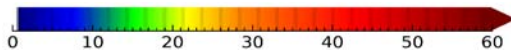
643

644

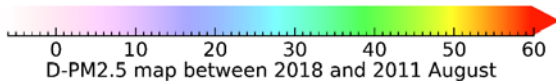
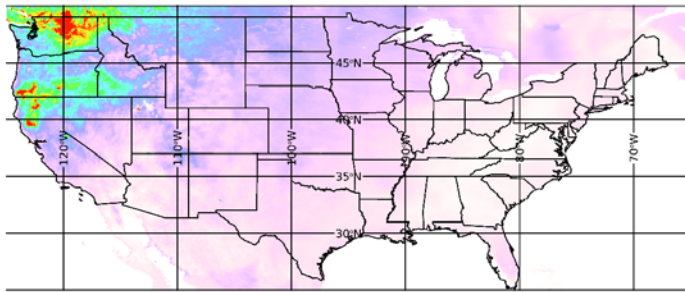
645



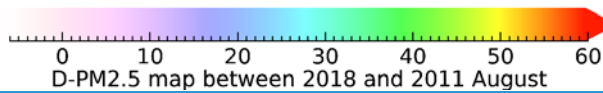
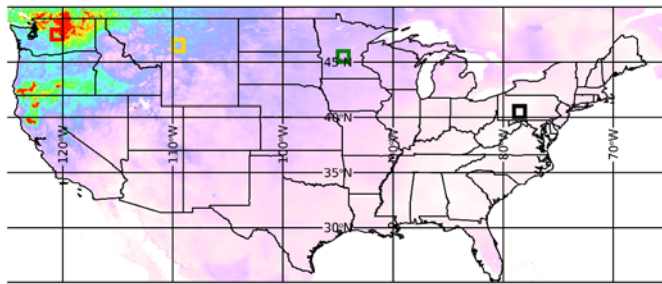
646



647



648



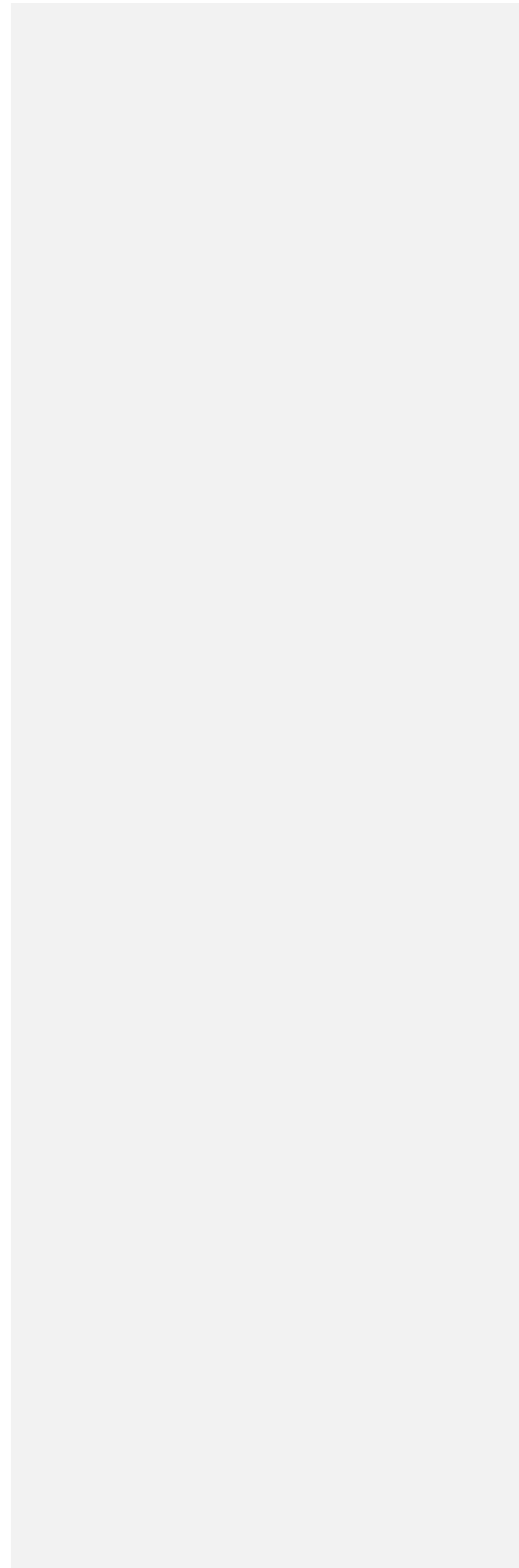
649

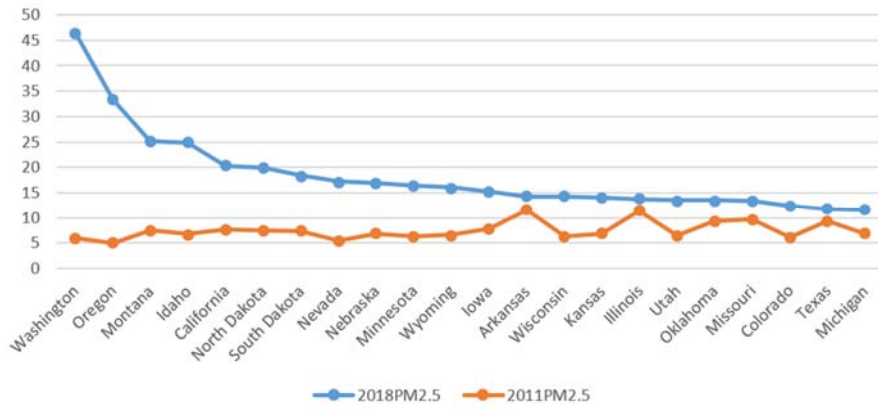
650 Figure 4. (a) EPA ground observed PM2.5 distribution over the US averaged from August 9th to
651 August 25th, 2018. (b) GWR predicted 17-day mean PM2.5 distribution. (c) Difference map of
652 predicted ground PM2.5 of the 17-day mean values between 2018 and 2011. PM2.5 values equal
653 or larger than $30 \mu g m^{-3}$ are shown as the same color (red). Note that the D-PM2.5 has a
654 different color scale to make the negative values more apparent (blue).

Xue, Gupta, Christopher, submitted to Remote Sensing of Environment

655

656





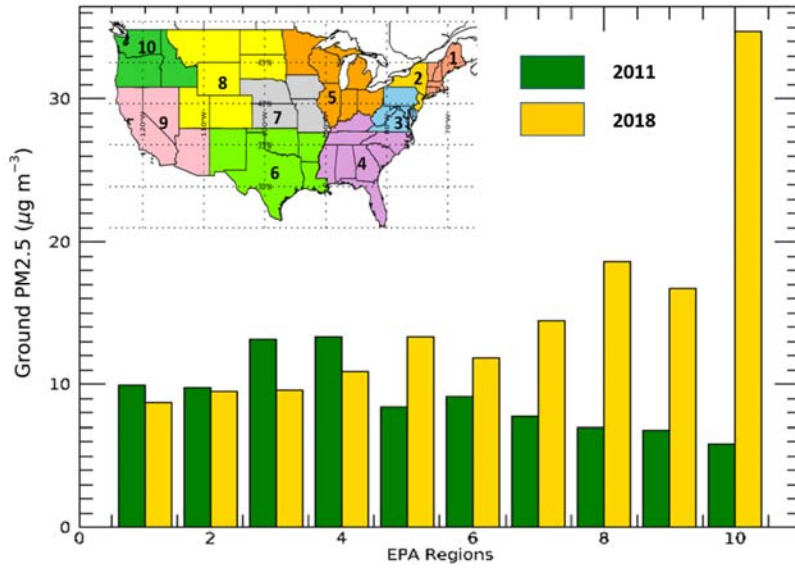
657

658

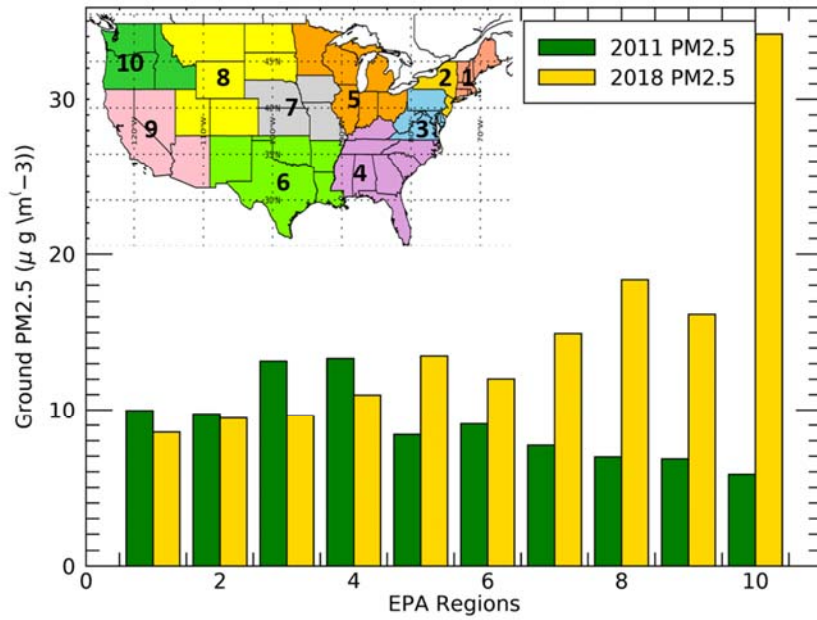
659

Figure 5. Mean PM2.5 from August 9th to August 25th in 2018 and 2011 of most affected states

Formatted: Centered



660



661
662 Figure 65. Mean PM2.5 of EPA regions from August 9th to August 25th in 2011 and 2018. Inset
663 shows the map of 10 EPA regions in different colors. Yellow column represents the 2018 mean
664 PM2.5 and green column represents for 2011 mean PM2.5.

665
666